

# Doubling the FOV of AR displays with a liquid crystal polarization-dependent combiner

KUN YIN,<sup>1</sup> ZIQIAN HE,<sup>1</sup> KUN LI,<sup>2</sup> AND SHIN-TSON WU<sup>1,\*</sup> 

<sup>1</sup>College of Optics and Photonics, University of Central Florida, Orlando, Florida 32816, USA

<sup>2</sup>Goertek Electronics, 5451 Great America Parkway, Suite 301, Santa Clara, CA 95054, USA

\*swu@creol.ucf.edu

**Abstract:** We propose a glasses-like augmented reality (AR) display with an extended field-of-view (FOV) using a liquid crystal polarization-dependent combiner (PDC). Such a PDC consists of two polarization volume lenses (PVLs) that are based on patterned liquid crystals to selectively control the beam path according to the right-handed or left-handed circularly polarized light. By encoding the left and right half of the FOV into two orthogonal polarization states, the overall horizontal FOV can be doubled while maintaining an ultrathin and flat form factor. Based on this multiplexing concept, the FOV can be further extended by integrating more PVLs with different diffraction angles. The proposed configuration with polarization-time multiplexing provides a promising solution for overcoming the limited FOV issue in AR displays.

© 2021 Optical Society of America under the terms of the [OSA Open Access Publishing Agreement](#)

## 1. Introduction

Augmented reality (AR) displays have found widespread applications in entertainment, education, engineering, and medical surgeries, just to name a few [1,2]. Through combining the computer-generated images with see-through environment, AR technology as an information platform is revolutionizing the relationship and interactions between viewers and displays. To provide a realistic viewing experience, various optical combiners have been developed, such as total-internal-reflection (TIR) freeform combiners [3], grating-based waveguide combiners [4–6], and free-space combiners [7]. Generally, the freeform combiners can achieve a wide field-of-view (FOV) but they suffer from large volume and sophisticated optical design [8,9]. On the contrary, the waveguide combiners possess a compact design but limited viewing angle due to the constrain of TIR [10]. Therefore, the free-space combiners with a sufficient FOV and high degree of design freedom have attracted increasing attention. Due to different working principles, free-space combiners can be further divided into two categories: reflective and diffractive combiners [11]. Among them, the diffractive free-space combiner with a thin form factor and lightweight is more favorable in the current stage to satisfy the need for glasses-like AR devices.

More specifically, such a diffraction-type free-space combiner is generally realized by holographic optical elements with imaging capability [12]. Based on different system designs, the computer-generated image will be displayed at a designated depth or at infinity. The FOV is dependent on the system design, such as the viewing angle of the combiner lens. To extend the viewing angle, reducing the  $f$ -number of the combiner lens is an effective and straightforward approach. However, when the  $f$ -number of an off-axis lens is reduced, the imaging aberrations become more serious [13]. Therefore, expanding the FOV becomes one of the most pressing challenges in a glasses-like AR system. Recently, a novel polarization volume lens (PVL) based on liquid crystal (LC) has been developed [14]. Based on the self-organized structure, PVLs possess several unique properties, such as strong polarization selectivity, large off-axis angle, and simple fabrication process. In addition, liquid crystals exhibit a higher refractive index than conventional photopolymers employed in holographic optical elements. Aside from advances in combiner lens, the optical system design with polarization multiplexing concept has also been

proposed with metagratings [15] and successfully implemented in the waveguide-based AR system using polarization gratings [16].

In this paper, we demonstrate a glasses-like AR system with a novel polarization-dependent combiner (PDC) to expand the FOV. This concept is analogous to the polarization division multiplexing in optical fiber communications, where two orthogonal polarizations are used to double the information capability. Here, we extend the viewing angle by presenting the left and right FOVs into two orthogonal polarization states, left-handed and right-handed circularly polarized (LCP and RCP) light, respectively. The PDC consisting of two PVLs with opposite polarization response and different off-axis angles, is designed to selectively diffract LCP and RCP images. By using an optical engine and a liquid crystal polarization modulator (LCPM) to create two images with orthogonal polarization states, the proposed AR configuration exhibits an extended image content while maintaining a compact form factor.

## 2. Polarization-dependent combiner

In our system, PDC is a critical optical component, which can distinguish orthogonal polarization states while offering different responses. To meet these requirements, we propose a novel PDC consisting of two PVLs with opposite polarization responses and different diffraction angles. Figure 1(a) shows the PVL with a strong polarization selectivity (LCP or RCP) and imaging power [14]. The diffraction angle is denoted as  $\alpha$ . Specifically, the PVL is a patterned cholesteric liquid crystal (CLC) device with a designed lens profile. By following the alignment pattern (Fig. 1(b)) on the bottom surface, CLC molecules continuously and periodically rotate in the  $xy$ -plane and twist along a tilted helical axis (Fig. 1(c)) in the  $xz$ -plane. The off-axis angle and focal length of PVL can be controlled by tuning the phase change on surface patterning, which is determined by the interference exposure during fabrication process. Moreover, PVLs possess a large diffraction angle and potentially a small  $f$ -number. Besides, PVL is a polymerized ultrathin film (from hundreds of nanometers to several microns) with controllable diffraction efficiency. Here, we stack two PVLs (PVL-L and PVL-R) with opposite polarization responses as the PDC. As shown in Fig. 1(d), the PVL-R responds to RCP light while PVL-L diffracts the LCP light with a different angle. Due to the thin film form factor, the combined PDC can increase the polarization responses while keep an ultrathin profile.

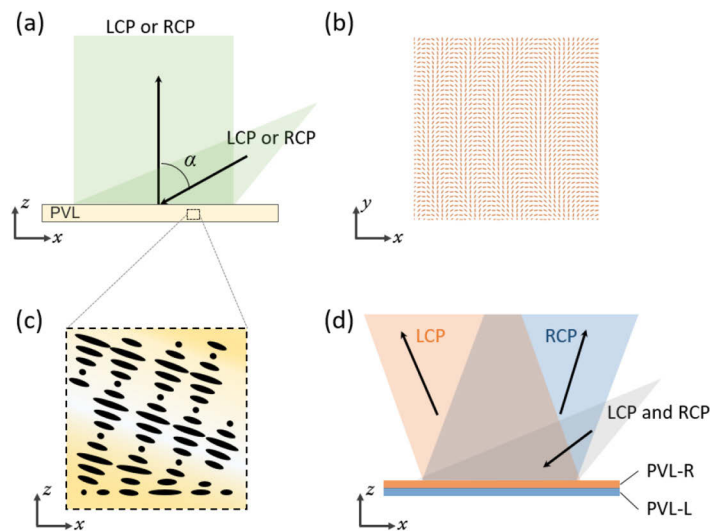


**Fig. 1.** Schematic illustrations of (a) a PVL with (b) surface alignment and (c) CLC structure. (d) Schematic diagram of the PDC with two combined PVLs.

### 3. Polarization-time multiplexing system configuration

A typical device configuration of free space AR systems with a diffractive combiner is shown in Fig. 2(a) [12]. The system usually has a pupil-forming design. The image is first projected into space by a relay optics, and then the intermediate image is delivered to viewer's eye with the diffractive combiner. The depth and size of the virtual image can be controlled by changing the distance between the intermediate image and the combiner lens.

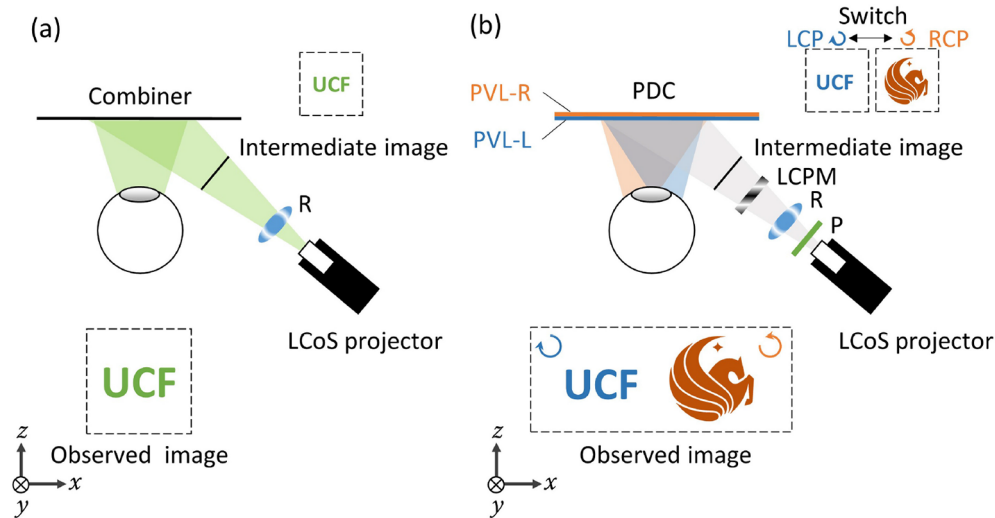


**Fig. 2.** Schematic illustrations of (a) a free space AR system and (b) a polarization-time multiplexing free space AR system. R: relay optics; P: polarizer; LCPM: liquid crystal polarization modular; PDC: polarization-dependent combiner.

To expand the FOV, here we propose a polarization-time multiplexing system based on two orthogonal polarization states to tile the left and right images together. Figure 2(b) depicts the system configuration. The optical engine in the system can be a conventional 2D display, such as a liquid-crystal-on-silicon (LCoS) or a digital light processing (DLP) projector. Without losing generality, we add a polarizer in front of the optical engine to make the emitted light with linear polarization in  $xz$ -plane ( $0^\circ$ ). Then an LCPM, aligned after the polarizer, is designed to obtain modulation between two orthogonal polarization states, namely  $0^\circ$  (in  $xz$ -plane) and  $90^\circ$  (along  $y$ -axis). With an integrated  $\lambda/4$  plate oriented at  $45^\circ$ , these two orthogonal linear polarizations would be converted to LCP and RCP waves, respectively. When switching the computer-generated sub-frame images in the time domain, the LCPM can offer corresponding polarization state for each sub-frame simultaneously. Due to time multiplexing, the final refresh rate of the system should be taken into consideration. Generally, the switching between each sub-frame can be determined by the number of frames, response time of the LCPM, and the frame rate of the LCoS. The response time of LCPM is usually between 1 ms (1 kHz) and 4 ms (250 Hz), depending on the material and cell gap employed. The number of sub-frames is two. Therefore, if the refresh rate of LCoS is 240 Hz, the final system refresh rate will be 120 Hz. For example, as shown in Fig. 2(b), when the displayed content is a school logo (Pegasus), the LCPM will be turned on so that it will synchronize the polarization to RCP. When the optical engine switches the content to letters (UCF), then the LCPM will switch the corresponding polarization to LCP. That is to say, the LCPM and the optical engine jointly control the polarization state and content of the intermediate image. However, how to input the intermediate image to the PDC needs to be carefully considered. Let assume the focal length of PVL-L and PVL-R is  $f_L$  and  $f_R$ ,

respectively, and the angle between the incident beam and the normal direction of the PDC is  $\theta$ . To diffract two images into left and right, the diffraction angle of PVL-L and PVL-R should be  $\theta + \varphi_L$  and  $\theta - \varphi_R$ , respectively. When the intermediate image is placed at a distance  $d_{1-L}$  from PVL-L, the image distance  $d_{2-L}$  can be estimated by the thin lens conjugate equation:

$$d_{2-L} = \frac{f_L d_{1-L}}{f_L + d_{1-L}}, \quad (1)$$

here distance  $d_{2-L}$  is the approximate depth of the observed virtual image from human eye. The size of the virtual image  $A_{2-L}$  should be:

$$A_{2-L} = AM_L = A_1 \frac{d_{2-L}}{d_{1-L}}, \quad (2)$$

where  $A_1$  stands for the size of the intermediate image and  $M_L$  is the magnification of the PVL-L. The same goes for the PVL-R. It is worth mentioning that the perceived image depths from two PVLs must be matched to tile the retina image smoothly, as Fig. 2(b) illustrates. Thus, the image distance  $d_{2-L}$  and  $d_{2-R}$  should be the same, namely  $d_2$ , and the  $A_2$  will also be the same. In addition, there can be some space between the two virtual images, but they cannot overlap. Therefore, the overall horizontal FOV can be generally expressed as:

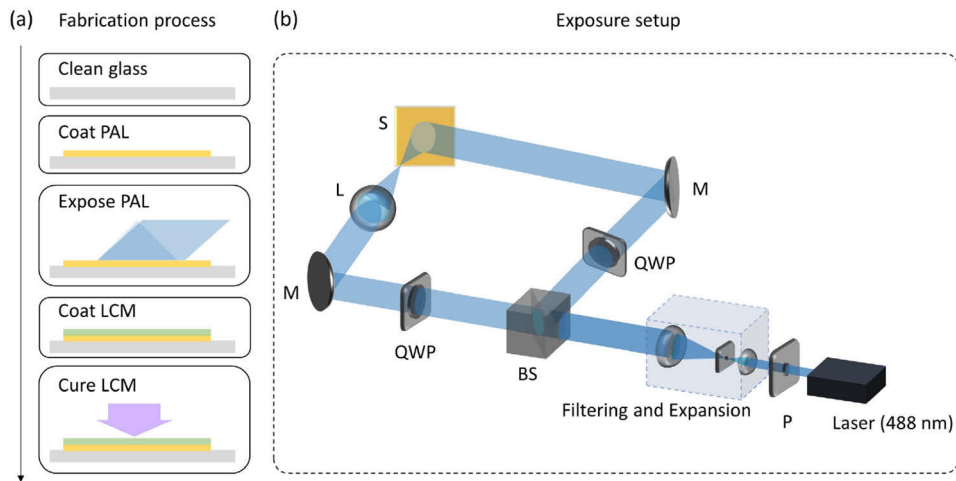
$$FOV = \arctan\left(\frac{A_2}{2d_2} + \tan \varphi_L\right) + \arctan\left(\frac{A_2}{2d_2} + \tan \varphi_R\right). \quad (3)$$

If the two images are symmetrically and perfectly tiled without any space, then the horizontal FOV can be simplified as  $FOV = 2\arctan(A_2/d_2)$ . The vertical FOV is limited by the viewing angle of each PVL. Generally, the vertical viewing angle is the same as the horizontal one before multiplexing. Therefore, the simplified diagonal FOV can be calculated as  $FOV = \sqrt{5}/2 \arctan(A_2/d_2)$ . Based on this equation, if we apply a larger intermediate image, then a wider FOV can be obtained. Moreover, it is worth mentioning that the eyebox should be the overlapping area of the two polarization paths. This area can be further enlarged when the eye relief is decreased, the size of the intermediate image is increased, or the divergence angle of the two paths is reduced.

#### 4. Experiment

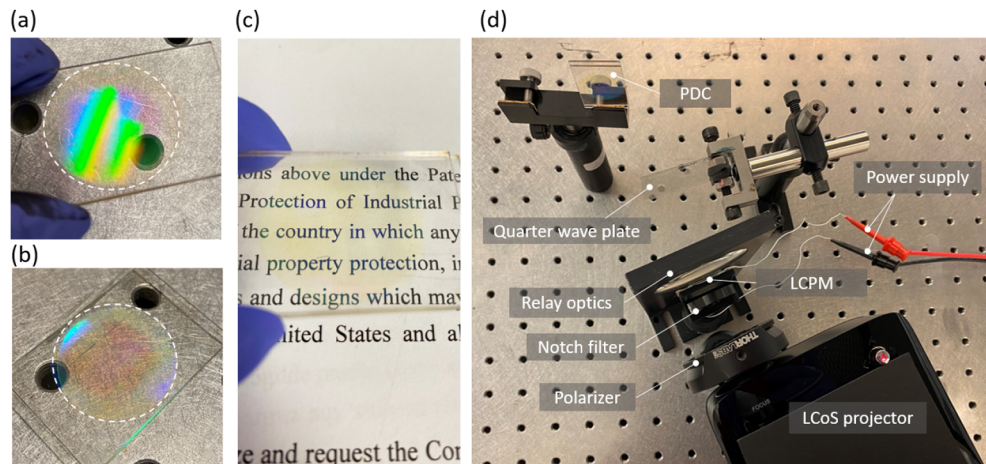
In this section, we show our experimental setup and demonstrate an example for doubling the FOV design discussed above. The system basically follows the layout shown in Fig. 2(b). In our experiments, a computer-controlled LCoS projector (LG-PH150B) was employed as the optical engine. The PDC consists of two PVLs: PVL-L responding to LCP and PVL-R to RCP, respectively. Generally, the distance between the side image and the combiner is around 3 cm to 5 cm, and the angle between the incident beam and the viewer is around  $30^\circ$  to  $70^\circ$ . Based on the consideration of the real case, for PVL-L, its focal length is  $f_L = 3$  cm and off-axis angle is  $52^\circ$ , while for PVL-R its focal length is  $f_R = 3$  cm and off-axis angle is  $27^\circ$ . Both PVLs were fabricated following the procedure shown in Fig. 3(a). First, a thin film of photoalignment (PA) material (BY, Brilliant Yellow from Tokyo Chemistry Industry) was spin-coated onto a cleaned glass. Then, the substrates with BY coating were mounted on the exposure setup (Fig. 3(b)) to record the surface alignment patterns. After exposure, the liquid crystal mixture (LCM) with opposite chiral dopant, R5011 and S5011, was spin-coated for the PVL-L and PVL-R, respectively. Finally, the samples were polymerized by a UV lamp. More detailed operation principles and fabrication procedures of the PVL can be found in [14,17].

Figure 4(a) shows a photo of the fabricated PVL-R, which is circled by the white dashed lines and the lens surface is clear and uniform. The green images observed are the ceiling fluorescent lamps in our lab. The other colors are the dispersion from this diffractive lens. Next,



**Fig. 3.** (a) PVL fabrication workflow. (b) Exposure setup for recording the surface pattern. (PAL: photoalignment layer; LCM: liquid crystal mixture; P: polarizer; SLM: spatial light modulator; QWP: quarter-wave plate; L: template lens; S: sample).

we fabricated PVL-L and laminated it with PVL-R together using a UV optical glue (NOA65), as Fig. 4(b) shows. The PDC region is circled by the white dashed lines. The thickness of each PVL is  $\sim 1 \mu\text{m}$ , and the total thickness of PDC, including the substrates, is 1 mm. The text shown in Fig. 4(c) is imaged through the sample. The distance between PDC and camera is 5 cm, and the target is 7 cm away. The clear image seen through the PDC region indicates the combiner exhibits a relatively high transmittance and negligible scattering. Due to the color of the employed photoalignment material (Brilliant Yellow), the sample appears yellowish, but this can be eliminated by using a colorless photo-alignment material.



**Fig. 4.** Photo of (a) the fabricated PVL-L and (b) the PDC consisting of PVL-L and PVL-R. (c) A photo taken through the PDC sample, where the PDC region is yellowish. The distance between PDC and camera is 5 cm, and the target is 7 cm away. (d) Experimental setup.

To prepare the LCPM, we filled a liquid crystal (MLC-6686, Merck) into a commercial twisted nematic (TN) cell (cell gap  $d=4.9 \mu\text{m}$ ) and an AC voltage is applied to control the on and off

states. Normally, the voltage is  $5 V_{\text{rms}}$ , depending on the employed LC material and cell gap. Then we used a broadband quarter-wave plate to convert the linearly polarized light into circularly polarized light. The whole experimental setup was constructed on an optical table. As captured in Fig. 4(d), a positive lens with focal length  $f = 12$  cm was used as the relay optics in our experiments. A camera was placed in front of the PDC to capture the displayed images. To eliminate the ghost images generated by the dispersion from diffractive optics, we added a notch filter (NF533-17 from Thorlabs) after the polarizer.

Figure 5 shows the experimental results. The intermediate image is 2.9 cm away from the PDC. The angle between the input beam and the normal of the PDC is about  $40^\circ$ . When we turn the LCPM on, there will be only LCP light. The viewing angle of LCP alone is about  $26^\circ$  with showing UCF letters, as illustrated in Fig. 5(a). Due to the large off-axis imaging, we can see the obvious distortion, especially for the letter U. This optical aberration can be mitigated through pre-processing the input contents, but this will bring more burdens to both computation and information transforms [14]. By switching the LCPM from on to off state, we can observe the RCP image. As depicted in Fig. 5(b), the viewing angle is  $23^\circ$  with showing school logo. Then we simultaneously switch the LCPM and the computer-generated images to observe the combined image. As expected, in Fig. 5(c), the overall horizontal FOV is dramatically extended to  $50^\circ$ . Although the PDC's diffraction efficiency for LCP mode is slightly lower than that for RCP, the intensity for each polarization channel can be improved by controlling the film thickness or pre-image processing compensation. Moreover, the proposed method can display full-color images by utilizing multilayered PVLs with red, green, and blue responses, respectively. To avoid crosstalk between each PVL, a narrowband image source is preferred.

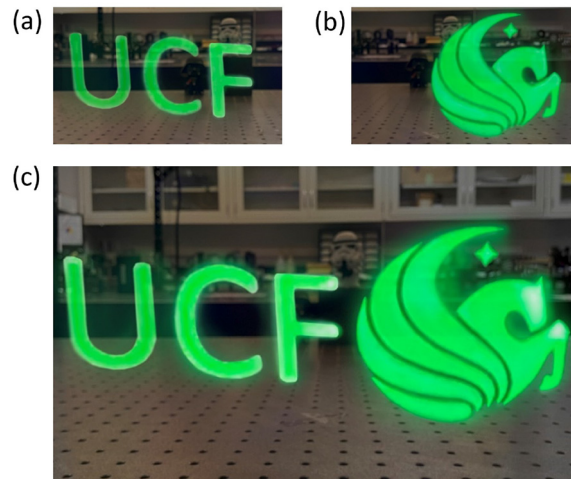


**Fig. 5.** (a) Captured image of LCP light, UCF. (b) Captured image of RCP, school logo. (c) Captured image of the combined images.

## 5. Discussion

In our demonstration, we use a novel PDC with two opposite polarization responses to achieve an extended FOV. In order to further improve the functionality based on the polarization-time multiplexing system, both the number of sub-frames and the PDC can be optimized [18]. In our proposed system, although there are only two orthogonal polarization states, the number of image channels can be further increased without being limited by the number of orthogonal polarizations. As depicted in Fig. 6(a), the image contents can be encoded into more than  $N$

channels ( $N \geq 3$ ) with the help of an improved PDC composed of active half-wave plates (HWPs) and PVLs. Each active HWP can be switched between on and off states to provide PVLs with the corresponding polarized light. Due to the requirement of single-polarization incidence, the LCPM can be simplified as a QWP to offer LCP or RCP light. More specifically, as an example illustrated in Fig. 6(b), when an incident light is RCP, the first HWP is turned on to convert RCP to LCP. The LCP light is diffracted by the first PVL-L. The image content is delivered to the viewer's eye. If the first HWP keeps at off state with the RCP incidence, the light will pass through the HWP and the first PVL-L, then encounter the second HWP with on state. The RCP will be converted to LCP and diffracted by the second PVL-L with a different diffraction angle. By analogy, PVLs of different angles can be stacked layer by layer. Figure 6(c) illustrates the image from each PVL with different diffraction angles. Moreover, this multiplexing system can be applied to expanding the vertical FOV as well. The image content can be encoded and then tiled in  $xy$ -plane instead of only along  $x$ -axis. To accommodate a large incident angle, a phase compensation film is usually required to keep the HWP working properly. Otherwise, multiple ghost images could be observed. Moreover, if the LCP light is not completely diffracted by the working PVL-L, then the remaining light will be further imaged by the following PVLs, which in turn generates ghost images. To overcome this issue, the HWP behind the working PVL-L can be turned on to convert the LCP light back to RCP.

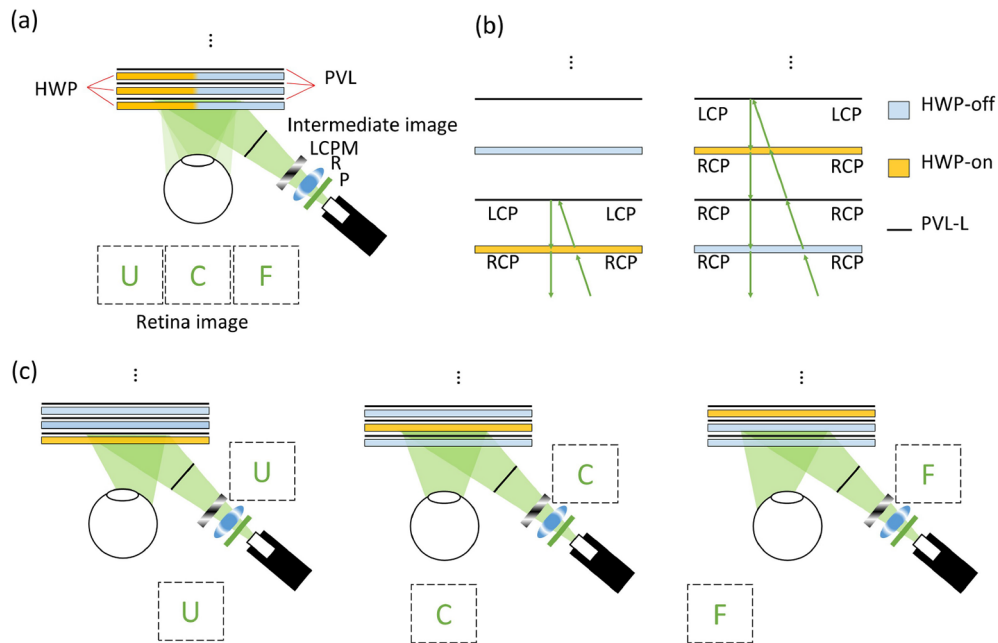


**Fig. 6.** Schematic illustrations of (a) an improved polarization-time multiplexing AR system (HWP: half-wave plate; R: relay optics; P: polarizer; LCPM: liquid crystal polarization modular; PDC: polarization-dependent combiner) with (b) a PDC composed of active HWP and PVLs. (c) Schematic illustrations of the image from each PVL.

## 6. Conclusion

We propose and demonstrate a polarization-time multiplexing system to double the FOV of a glasses-like AR display. The multiplexing is achieved by PDC, which is composed of two PVLs with orthogonal polarization responses. In experiment, a PDC is fabricated using patterned CLC polymers which can achieve high uniformity and negligible scattering. By constructing

the proposed system with an electronically controlled LCPM, the enlarged overall horizontal FOV = 50° is achieved. To further improve the system, we optimize the PDC with active HWPs. By stacking the layer of active HWPs and PVLs, we can theoretically obtain an ultra-wide FOV by tiling multiple sub-frame images based on the polarization-time multiplexing system. In summary, we show a promising approach to achieve wide FOV in glasses-like AR displays while keeping a simple system configuration.

**Funding.** Goertek Electronics.

**Disclosures.** The authors declare no conflicts of interest.

## References

1. O. Cakmakci and J. P. Rolland, "Head-worn displays: A review," *J. Disp. Technol.* **2**(3), 199–216 (2006).
2. T. Zhan, K. Yin, J. Xiong, Z. He, and S. T. Wu, "Augmented reality and virtual reality: perspectives and challenges," *iScience* **23**(8), 101397 (2020).
3. H. Huang and H. Hua, "High-performance integral-imaging-based light field augmented reality display using freeform optics," *Opt. Express* **26**(13), 17578–17590 (2018).
4. K. Yin, H. Y. Lin, and S. T. Wu, "Chirped polarization volume grating for wide FOV and high efficiency waveguide-based AR displays," *J. Soc. Inf. Disp.* **28**(4), 368–374 (2020).
5. B. Kress, "Optical waveguide combiners for AR headsets: features and limitations," *Proc. SPIE* **11062**, 17 (2019).
6. Y. Weng, Y. Zhang, J. Cui, A. Liu, Z. Shen, X. Li, and B. Wang, "Liquid-crystal-based polarization volume grating applied for full-color waveguide displays," *Opt. Lett.* **43**(23), 5773–5776 (2018).
7. S. Lee, B. Lee, J. Cho, C. Jang, J. Kim, and B. Lee, "Analysis and implementation of hologram lenses for see-through head-mounted display," *IEEE Photonics Technol. Lett.* **29**(1), 82–85 (2017).
8. O. Cakmakci and J. Rolland, "Design and fabrication of a dual-element off-axis near-eye optical magnifier," *Opt. Lett.* **32**(11), 1363–1365 (2007).
9. H. Hua, X. Hu, and C. Gao, "A high-resolution optical see-through head-mounted display with eyetracking capability," *Opt. Express* **21**(25), 30993–30998 (2013).
10. K. Yin, H. Y. Lin, and S. T. Wu, "Chirped polarization volume grating with ultra-wide angular bandwidth and high efficiency for see-through near-eye displays," *Opt. Express* **27**(24), 35895–35902 (2019).
11. Y. H. Lee, T. Zhan, and S. T. Wu, "Prospects and challenges in augmented reality displays," *Virtual Reality & Intelligent Hardware* **1**(1), 10–20 (2019).
12. J. Xiong, K. Yin, K. Li, and S. T. Wu, "Holographic optical elements for augmented reality: principles, present status, and future perspectives," *Adv Photo Res* **2**(1), 2000049 (2021).
13. H. Peng, D. Cheng, J. Han, C. Xu, W. Song, L. Ha, J. Yang, Q. Hu, and Y. Wang, "Design and fabrication of a holographic head-up display with asymmetric field of view," *Appl. Opt.* **53**(29), H177–H185 (2014).
14. K. Yin, Z. He, and S. T. Wu, "Reflective polarization volume lens with small f-number and large diffraction angle," *Adv. Opt. Mater.* **8**(11), 2000170 (2020).
15. Z. Shi, W. T. Chen, and F. Capasso, *Proc. SPIE* **10676**, 1067615 (2018).
16. C. Yoo, K. Bang, M. Chae, and B. Lee, "Extended-viewing-angle waveguide near-eye display with a polarization-dependent steering combiner," *Opt. Lett.* **45**(10), 2870–2873 (2020).
17. K. Yin, J. Xiong, Z. He, and S. T. Wu, "Patterning Liquid Crystal Alignment for Ultra-Thin Flat Optics," *ACS Omega* **5**(49), 31485–31489 (2020).
18. L. Lu, F. Peng, and D. Lanman, "Varifocal system using hybrid tunable liquid crystal lenses," U.S. patent 16,271,344 (January 30, 2020).